Available online at www.sciencedirect.com

SCIENCE DIRECT®

PERGAMON

International Journal of Multiphase Flow 29 (2003) 341–360

International Journal of Multiphase Flow

www.elsevier.com/locate/ijmulflow

Two-phase flow patterns in parallel micro-channels

G. Hetsroni *, A. Mosyak, Z. Segal, E. Pogrebnyak

Department of Mechanical Engineering, Technion—Israel Institute of Technology, Haifa 32000, Israel

Received 9 September 2002; received in revised form 12 December 2002

Abstract

Micro-channel heat sinks with two-phase flow can satisfy the increasing heat removal requirements of modern micro-electronic devices. Some of the important aspects associated with two-phase flows in micro-channels, is to study the bubble behavior and flow regimes in diabatic, parallel micro-channels. Most of the reports in the literature present data of only a single channel and mostly adiabatic. This does not account for flow mixing and hydrodynamic instability that occurs in parallel micro-channels, connected by common inlet and outlet collectors. In the present study, experiments were performed for air–water and steam–water flow in parallel triangular micro-channels. The experimental study is based on systematic measurements of temperature and flow pattern by infrared radiometry and high-speed digital video imaging. In air–water flow different flow patterns were observed simultaneously in the various micro-channels at a fixed values of water and gas flow rates. In steam–water flow, instability in uniformly heated micro-channels was observed. This work develops a practical modeling approach for two-phase micro-channel heat sinks and considers the discrepancy between flow patterns of air–water and steam–water flow in parallel micro-channels.

Keywords: Two-phase flow; Heat transfer; Micro-channels; Dryout

1. Introduction

Various aspects of two-phase flow and change-of-phase heat transfer in micro-channels have been investigated recently including two-phase flow patterns, Damianides and Westwater (1988); Fukano and Kariyasaki (1993); Triplett et al. (1999); Zhao and Bi (2001), and two-phase heat transfer Peng and Wang (1998); Peng et al. (1998); Hetstroni et al. (2001); Zhang et al. (2002); Kandlikar (2002).

* Corresponding author. Tel.: +972-4-8292058; fax: +972-4-8238101.
E-mail address: hetsroni@techunix.technion.ac.il (G. Hetsroni).

0301-9322/03/$ - see front matter
doi:10.1016/S0301-9322(03)00002-8

Recently published research dealing with gas–liquid two-phase flow in micro-channels is reviewed by Ghiaasiaan and Abdel-Khalik (2001). Only micro-channels with hydraulic diameters of the order of 0.1–1 mm and with large length-to-hydraulic diameter ratios were considered. That review is restricted to situations where the fluid inertia is significant in comparison with surface tension.

Previous studies on heat transfer to a two-phase capillary flow in a heated micro-channel provide estimates of the effects of capillary, inertia, friction and gravity forces on the velocity distribution and temperature field along a single capillary (Ory et al., 2000). However to provide effective cooling, a set of parallel micro-channels should be used rather than a single channel. Two-phase flow in parallel pipes, for which the feed is from a common manifold, displays interesting phenomena, as two phases may split unevenly when entering the parallel piping. Ozawa et al. (1979, 1989) performed experimental studies on two-phase flow systems in parallel pipes of 3.1 mm diameter. They simulated the flow in boiling channels by injection of air and water into the pipes. Their conclusion was that the injection of air has a destabilizing effect on pressure drop oscillations. On the other hand, the injection of liquid has a stabilizing effect, but includes a small-amplitude oscillation in the liquid flow rates. It would be interesting to see the effect of heat transfer during flow boiling in micro-channels.

The aim of the present study is to compare flow regimes in air–water flow to flow regimes in steam–water flow. Flow boiling in parallel micro-channels raises fundamental questions: how does the small-passage dimension affect the bubble dynamics and the two-phase flow; how is the temperature distribution on the heated surface affected at constant heat flux. Parallel triangular channels with the common inlet and outlet collectors were used. The experimental study is based on systematic observations and measurements by infrared radiometry and high-speed video images.

2. Experiments

Experimental apparatus. The experimental test facility and flow loop, for liquid flowing through micro-channels is shown in Fig. 1. It consists of peristaltic pump, pipes, test module, entrance and exit tanks. Working liquid (water at constant temperature) was pumped from the entrance tank through the inlet plenum, through the micro-channels in the test module, outlet plenum to the exit tank. The flow rate of the working fluid was controlled by adjusting the frequency of the peristaltic pump and was measured by a weighing method.

The flow visualization technique and the visualization of the thermal field at the heated wall is shown in Fig. 2. The motion of vapor–liquid flow in the micro-channels was studied using a microscope and high-speed video camera with recording rate up to 10,000 fps. The playback speed can be varied from a single frame to 250 fps. The IR radiometer has a sensitivity of 0.1 K and a typical resolution of 256 pixels per line. With the radiometer one can obtain a quantitative thermal profile in the line mode, the average temperature in the area mode, and the temperature of a given point in the point mode. The frequency response of the radiometer is 25 fps. In the present study, the frequency of the bubble growth in the micro-channel is higher than that, hence we confined ourselves to measurements of temperature field, on the heated bottom of the test module, averaged over a time interval of 0.04 s.

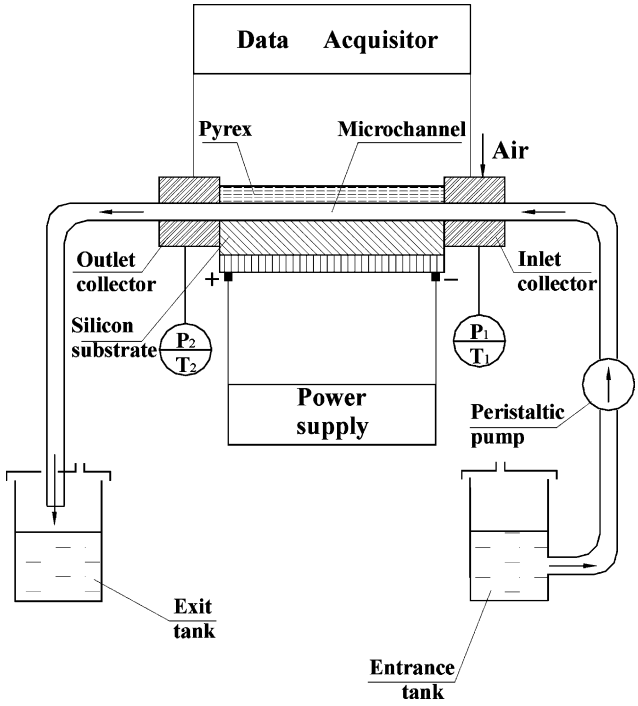

Fig. 1. Experimental apparatus.

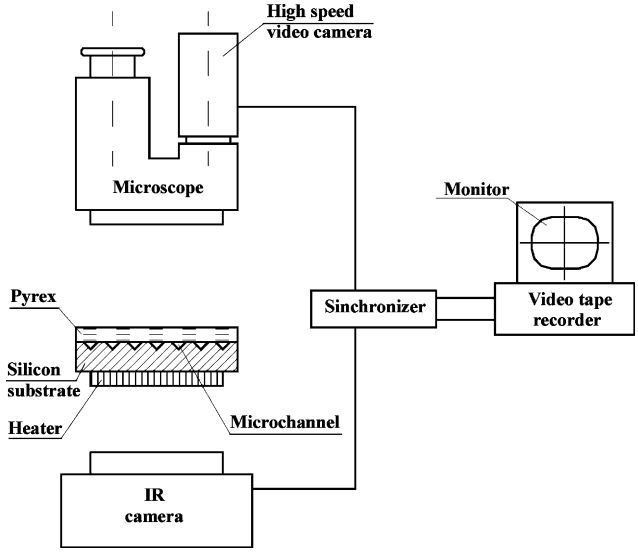

Fig. 2. Visualization technique.

The temperature of the working fluid was measured, at the entrance and exit of the test module, by 0.3 mm type-T thermocouples, with an accuracy of 0.1 K. Pressures were measured, at the inlet

and outlet of the test module, by silicon pressure sensors, with sensitivity 3.3 mV/kPa, response time 1.0 ms and accuracy of 1.5%. The flow rates of the working water and air were measured with an accuracy of 1% and 6%, respectively. The superficial water and air velocities were calculated with an accuracy of 2% and 7%, respectively. The vapor quality is calculated with an accuracy of 5–10% depending on the flow conditions.

Test sections. We have designed, manufactured and tested a number of prototypes that may be used in the thermal control of electronic devices. A typical test module is shown in Fig. 3. The test modules were fabricated of a square-shape silicon substrate 15×15 mm, 530 μm thick, and a Pyrex cover, 500 μm thick, which served as both an insulator and a transparent cover through which flow patterns and boiling phenomena could be observed. In the silicon substrate, parallel micro-channels were etched. The cross-section of each channel is an isosceles triangle with a base of 200–310 μm. The angles at the base are 55°. An electrical heater of 10×10 mm, made of a thin film resistor, was deposited on the surface of the silicon and served to simulate the heat source. The heater was connected to a DC power supply and heat generated in the heater was transferred to the liquid flow from the two sides of the triangular channels.

Although the channels were fabricated in such a way that the cross-section of all channels would be uniform, the flow rate through each channel may not be equal. The distribution of flow through the channels depends on the way of connection of the test section to the inlet and outlet collectors. Two types of connection were studied: type A shown in Fig. 4a and type B, shown in Fig. 4b. Type A provides the flow direction to the inlet plenum and from the outlet collector that is perpendicular to the flow direction in the micro-channels. Type B provides the same flow direction to the inlet and from the outlet collector as in the micro-channels. The geometry of the tested modules is given in Table 1.

Data reduction. The parameters used in the data reduction and analysis are summarized below:

Heat flux, q. In determination of the heat transferred from the heater to the working fluid, the heat losses due to conduction, convection and radiation were taken into account. The transferred heat was defined as $q = \varphi I(V/F)$ where I and V are input current and voltage, F is the heated area of the heater, φ is the ratio of the heat transferred to the working fluid to the total heat generation. For each set of steady-state experimental conditions the energy balance (based on the measurements of the inlet and outlet temperatures and calorimetric method) was performed and the value φ was calculated. The current data indicated that geometric parameters such as hydraulic diameter, design and material of the inlet and outlet collectors have a significant influence on the heat losses.

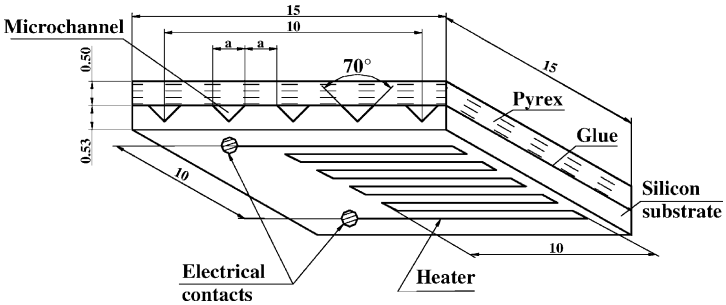

Fig. 3. Test section.

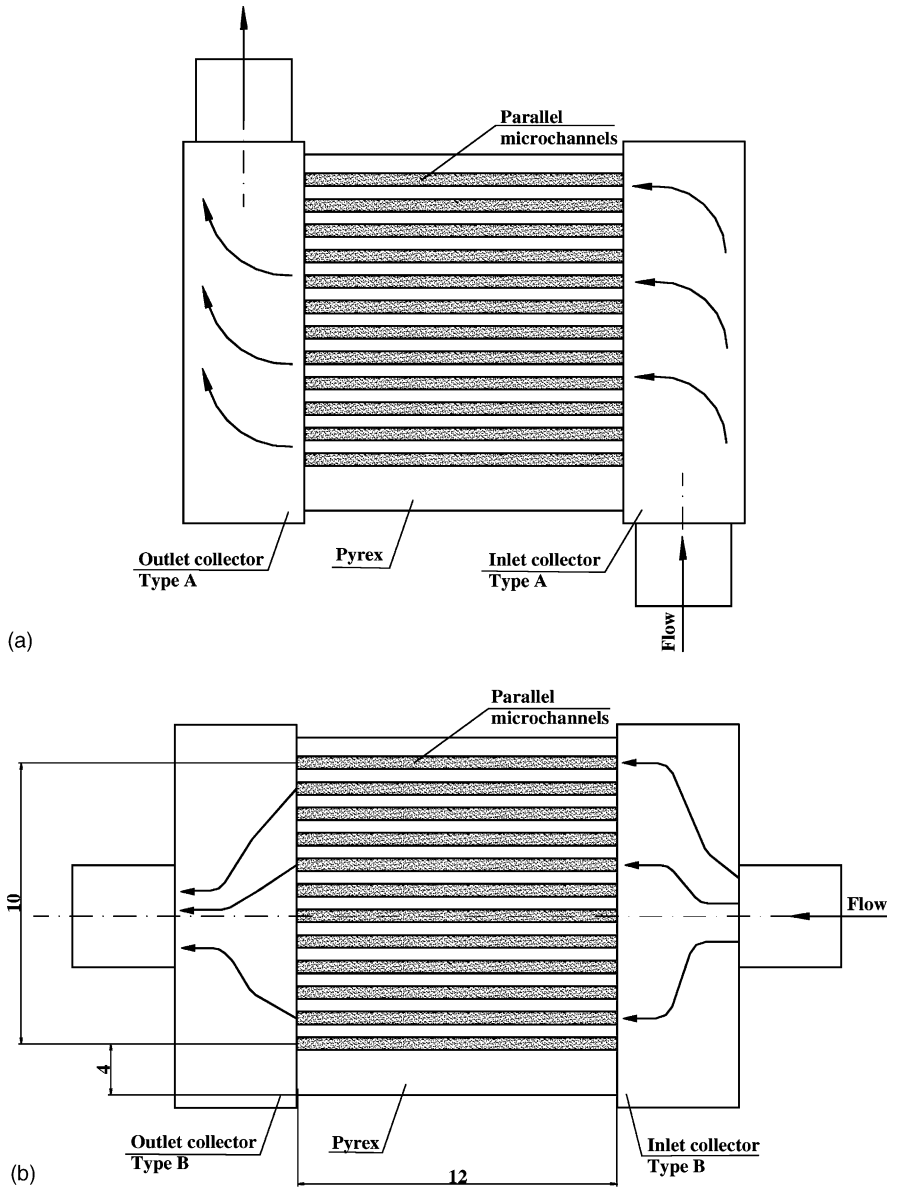

Fig. 4. Manifolds: (a) collector type A (b) collector type B.

Table 1
Geometry of test modules

Type of test module	Overall number of channels n	Channel hydraulic diameter, D_h (mm)	Type of plenum	Material of the plenum
1	21	0.129	A	Stainless steel
2	26	0.103	B	Plastic PEEC
3	17	0.161	A	Stainless steel

Table 2
Experimental conditions

Type of test module	Reynolds number	Heat flux (kW/m^2)	Irregularity of the heater temperatures T_{max}/T_{mean}
1	10–40	80–300	1.34–1.68
2	10–42	90–360	1.22–1.32
3	8–42	51–500	1.09–1.21

Reynolds number, $Re = UD_h/v$, where v is the kinematic viscosity, D_h is the hydraulic diameter, U is the mean flow velocity of the single-phase liquid. The kinematic viscosity was calculated using the temperature of the fluid at the inlet collector (Ghiaasiaan and Abdel-Khalik, 2001). The experimental conditions are given in Table 2.

- Mass velocity of the single-phase flow, $\dot{m}$. The mass velocity was calculated as $\dot{m} = Q\rho/A_c$, where v is the volumetric flow rate, ρ is the fluid density and A_c is the overall cross-section area of the micro-channels;
- Mass vapor quality at the outlet plenum, x, was calculated from the equation of change in the enthalpy of a liquid–vapor system during evaporation in the micro-channels.

3. Results

3.1. Air–water flow

Flow patterns. At different flow condition, different flow patterns were observed which can now be classified, depending on the interfacial configuration according to Lowe and Rezkallah (1999): liquid alone (or single-phase flow), bubbly flow, slug flow, annular flow (gas core with a thin liquid film, gas core with a thick liquid film). In the parallel channels having common inlet and outlet collectors non-uniform distribution of working fluid occurs. Tshuva et al. (1999) investigated the splitting of adiabatic two-phase flow in a system of two parallel pipes with a common feed and common exit. The results showed that the flow was non-symmetric. In the present study we observed simultaneous different flow pattern, in different parallel micro-channels. This point is illustrated in Fig. 5 for superficial liquid velocity $U_{LS} = 0.13$ m/s and superficial gas velocities $U_{GS} = 0.63$, 1.7 and 3.1 m/s, respectively. In this figure four parallel channels of test module 3 can be seen, the flow moves from left to right. The field of view is 2.4 mm in the streamwise direction and 2.2 mm in the spanwise direction.

The "liquid alone" pattern showed no entrained bubbles or gas–liquid interface in the field of view. The capillary bubbly flow, the first channel of the upper part of the Fig. 5a is characterized by appearance of distinct non-spherical bubbles, generally smaller in the streamwise direction than at the base of the triangular channel. This flow pattern was also observed by Triplett et al. (1999) in the 1.097 mm diameter circular tube and by Zhao and Bi (2001) in the triangular channel of hydraulic diameter of 0.866 mm. This flow, referred by Zhao and Bi (2001) as "capillary bubbly flow", has the following characteristics (as seen from Fig. 5a): the gas bubbles are regularly

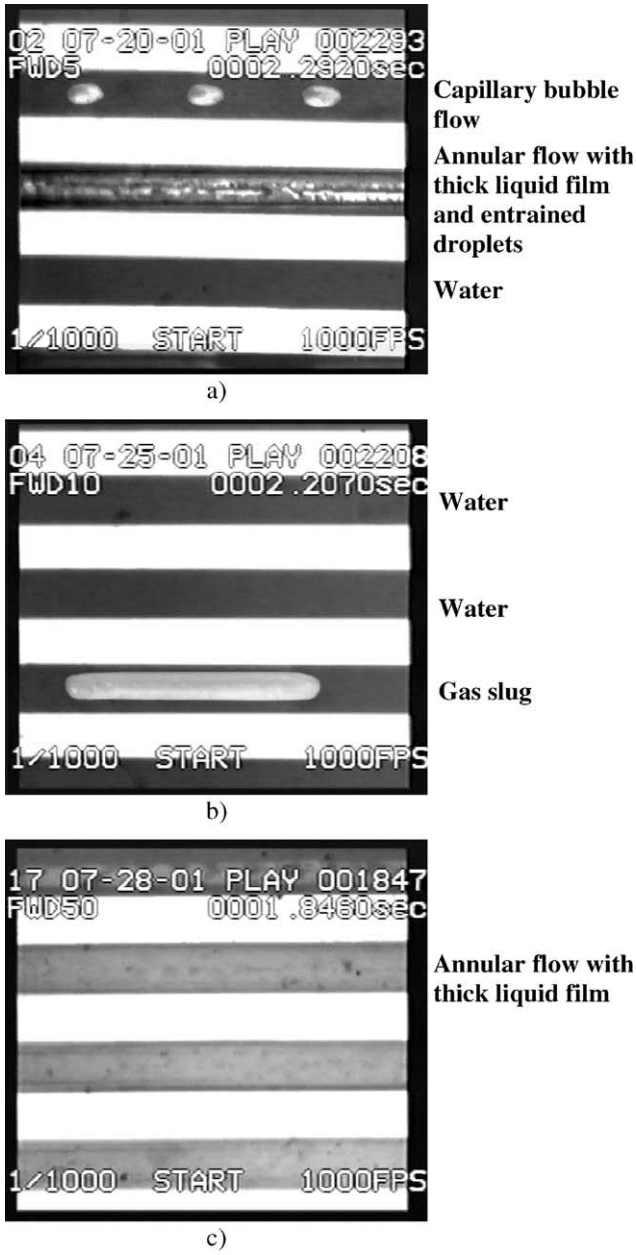

Fig. 5. Air–water flow in different parallel micro-channels. $U_{LS} = 0.13$ m/s. Type B plenum: (a) $U_{GS} = 0.63$ m/s; (b) $U_{GS} = 1.7$ m/s; (c) $U_{GS} = 3.1$ m/s.

distributed in the liquid phase, represented by a train of bubbles, essentially ellipsoidal in shape, spanning almost the entire cross-section with their centers located along the centerline of the channel.

The gas core with a thick liquid film is also shown in Fig. 5a (the second channel from the top). It is seen from this figure that liquid film formed at the side-walls of the channel with a continuous gas core in which a certain amount of liquid droplets exist. The flow with elongated cylindrical bubbles may be referred to "slug" flow, Fig. 5b (the third channel from the top). With increasing superficial gas velocity the gas core with a thin liquid film was observed. The flow pattern displayed in Fig. 5c (the second, third and fourth channels from the top) indicates that as the air velocity became high enough, the liquid droplets entrained in the gas core disappeared such that the flow became annular flow. Although the gas core may occupy almost the entire cross-section of the channel, making the side-walls partially dry, the liquid phase always remained continuous due to the fact that the liquid was drawn into the triangular corners by surface tension.

3.2. Steam–water flow

In parallel micro-channels, when heating is applied, vapor is generated, and the system may become unstable and often different flow regimes occur (Fig. 6).

Incipience of individual bubble. Predicting the incipient boiling is an integral part of a micro-channel heat sink design methodology. The ability to predict this condition is of paramount importance both as an upper design limit for heat sinks that are intended for single-phase cooling only, and as a lower limit for two-phase heat sinks intended for maximum heat dissipation. The present investigation focuses on a study of incipient boiling and bubble behavior at lower values of inlet liquid velocity. The experiments have shown the explosive bubble behavior. The location (along the test section) of the appearance of the first bubble at a given flow rate, depends on local surface temperature variation. Since the heated length of the test section is short (10 mm), at high values of the difference between maximum temperature on the heated wall, T_w^{max}, and saturation temperature T_S, significant interaction takes place between the steam generated and the feed water. It is very difficult to study the appearance of the first bubble at high values of $(T_w^{max} - T_S)$. We investigated this phenomenon under condition of $(T_w^{max} - T_S) = 6$ K, $q = 8 \times 10^4$ W/m^2, superficial liquid velocity $U_{LS} = 0.046$ m/s. In this case the beginning of bubble growth was observed close to the exit manifold.

The typical bubble behavior is shown in Fig. 7, (the second channel from the top) Fig. 7A and B illustrate the bubble shape at different instants of time during growth and motion. It is the top view, observed through the transparent cover. The field of view is 2.4 mm in the streamwise direction and 2.2 mm in the spanwise direction, the flow moves from left to right. In these images

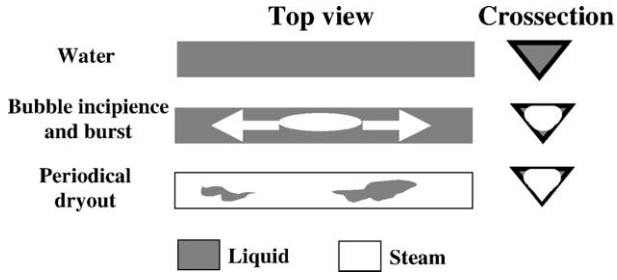

Fig. 6. Sketch of unstable flow regimes in steam–water flow.

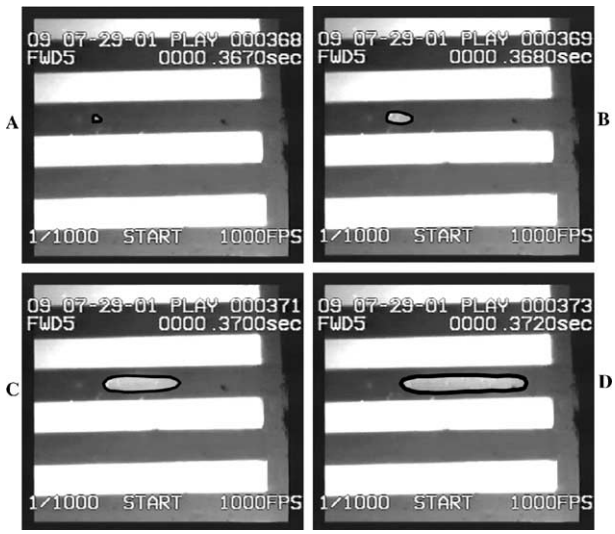

Fig. 7. Bubble growth. $U_{LS} = 0.046$ m/s, $q = 80$ kW/m^2. Type B plenum.

four micro-channels are shown marked by gray color or by gray color with the light regions. One can see that the vapor is generated in one micro-channel only. Fig. 7A shows the incipience of the bubble. The bubble is approximately spherical and occupies a small part of the triangular micro-channel. During 0.001 s it grows and occupies about 0.3 of the cross-section, Fig. 7B. At that point the bubble grows preferential in the axial direction, Fig. 7C. In Fig. 7C the bubble occupies about 0.7 of cross-section. Then the bubble moves into the exit manifold, Fig. 7D.

Bubble growth. When incipient boiling superheat is achieved, the vapor bubble nucleates and rapidly grows. The bubble is initially a small sphere and then the axisymmetric growth in a narrow channel takes place. Temporal variation of bubble size is shown in Fig. 8. Fig. 8a and b show variation of bubble size in the streamwise direction, D_p, and in the spanwise direction, D_n, respectively. From these figures one can conclude that at time $\tau = 0.375$ s the maximum length of the bubble in the streamwise direction, D_p, is about eight times larger than that in the spanwise direction, D_n.

The observed ratio $f = D_p/D_n$, is quite different from that reported for subcooled flow boiling of water in tubes of 17–22 mm inner diameter. Bibeau and Salcudean (1994); Prodanovic et al. (2002) reported that this ratio was typically around 0.8 for experiments at 1.05–3 bar. The situation considered in this paper is however different as the bubbles undergo a significant volume change and the flow is unstable. Ory et al. (2000) studied numerically growth and collapse of a bubble in a narrow tube filled with a viscous fluid. The situation considered in that study is also quite different from the present one as, in that case, heat was added to the system impulsively, rather than continuously as we do here.

Jiang et al. (2001) conducted visualization studies on boiling of water in triangular micro-channels with minimal width of 50 and 100 μm. At low heat fluxes, individual bubbles were observed growing and departing inside the micro-channels. Increasing the heat flux triggered an abrupt change in the flow pattern to an unstable slug flow. The interesting feature of this study is that the bubbly flow regime, common to macro-flow boiling systems, was never observed.

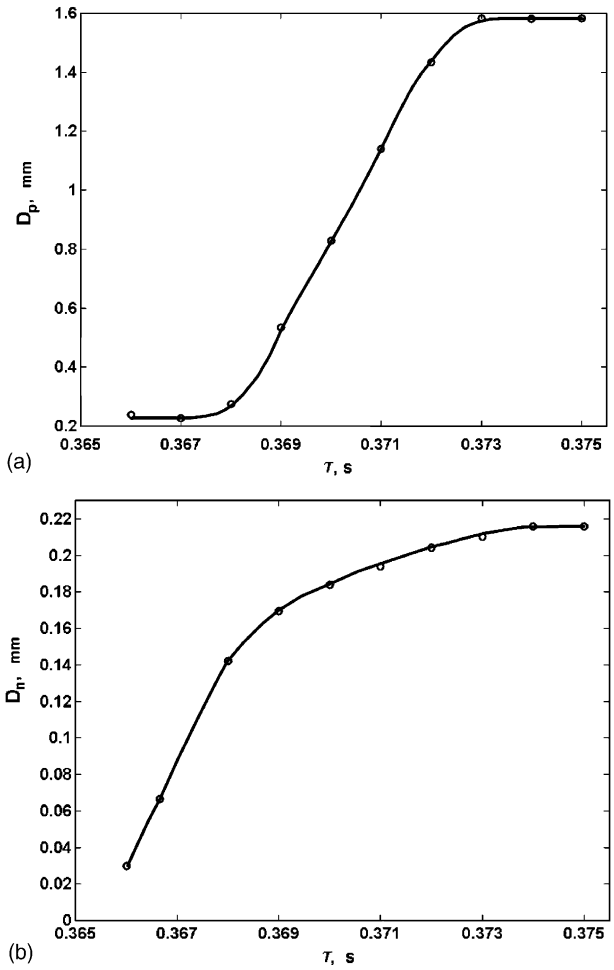

Fig. 8. Temporal variation of vapor bubble size: (a) streamwise direction, D_p (b) spanwise direction, D_n.

Kennedy et al. (2000) studied incipient boiling and onset of flow instability for subcooled water flow in uniformly heated micro-tubes with diameters of 1.17 and 1.45 mm. For smaller channels, significant deviation was found between experimental results and prior incipient boiling correlations. The observation made by these investigators shows that flow patterns, correlations and models available for macro-two-phase systems are unsuitable to micro-channel flow. Recently, an experimental investigation of the flow boiling of a liquid flowing through triangular micro-channels by Peng et al. (1998) showed that the wall superheat for the onset of boiling is very low. Qu and Mudawar (2002) performed experiments to measure the incipient boiling heat flux in a heat sink containing 21 rectangular (231 μm wide and 713 μm deep) micro-channels. Boiling incipience was identified when the first bubbles were detected growing at, and departing from, the micro-channel wall near the outlet. Tests were performed with inlet liquid velocities of 0.13–1.44 m/s. The incipient boiling heat flux and the incipient boiling superheat measured in the present study agree well with experimental data and model predictions reported by Qu and Mudawar (2002). One can conclude

that the model developed by Qu and Mudawar (2002) for rectangular channels may be adopted to predict the incipient boiling heat flux and the incipient boiling superheat for triangular channel as well.

Visual observation in the present study showed that the majority of the first bubbles were observed on the channel bottom wall, though a few bubbles did appear on the side-walls. After nucleation, bubbles first grew to detachment size before departing into the liquid flow. The detached bubbles moved to the downstream plenum.

Bubble velocity. Fig. 9 shows the velocity of displacement of the bubble tail in the streamwise direction, U_b (m/s), vs. bubble lifetime, τ, at fixed conditions as described above, i.e. $q = 8 \times 10^4$ W/m^2, $U_{LS} = 0.046$ m/s. One may conclude that the velocity of bubble displacement varies, depending on the given range of lifetime. In region A the boiling process during the time of about 0.005 s from the appearance of the first bubble, ONB, the bubble velocity is equal to the superficial liquid velocity. It should be noted that the term ONB, commonly known as the onset of nucleate boiling, was "borrowed" from the terminology of subcooled flow boiling in larger tubes. Region B is characterized by a sharp increase in the bubble velocity. One may conclude that the bubble is accelerated in the streamwise flow direction. Fig. 9 shows that in this region the bubble velocity increases about three-fold, during a time interval about 0.003 s. After the time when U_b reaches maximum value it remains constant, as shown in Fig. 9, region C.

Boiling in parallel micro-channels. Visual study. Fig. 10 illustrates two-phase flow, driven by a pump in the micro-channels of the test module. The vapor is generated only in part of the micro-channels and in different parts of the parallel micro-channels. In the micro-channels where vapor is generated two regions could be considered: one region, located close to the inlet collector, and the region located downstream from the inlet collector. Fig. 11 shows in detail the unsteady flow in one of the parallel micro-channels located close to the inlet plenum with heat flux, $q = 220$ W/m^2 and $U_{LS} = 0.14$ m/s. The flow moves from the left to the right, the field of view is about 0.7 mm in the streamwise direction and 1 mm in the spanwise direction. In Fig. 11a, single-phase water flow was mainly observed. An interesting phenomenon frequently happened, when the

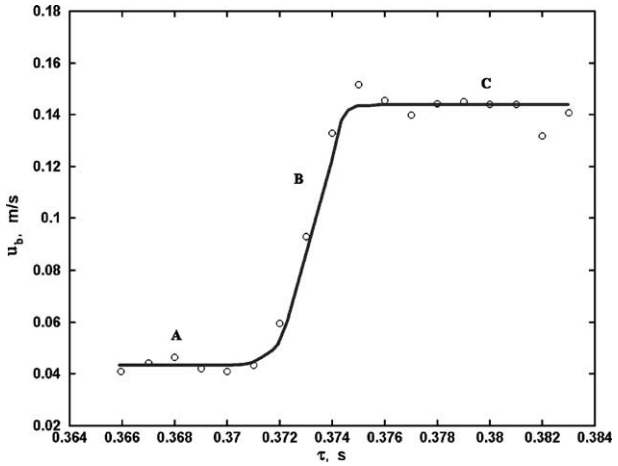

Fig. 9. Velocity of bubble displacement. $U_{LS} = 0.046$ m/s, $q = 80$ kW/m^2.

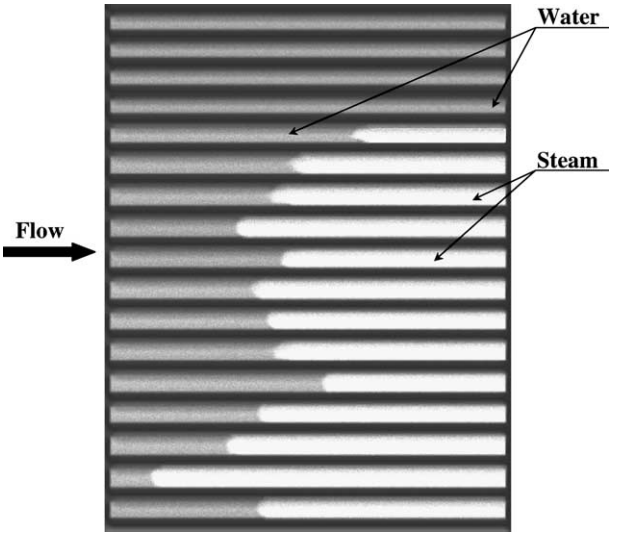

Fig. 10. Boiling in parallel micro-channels. Type A plenum.

applied heat flux or wall superheat was increased, clusters of vapor appeared as a jet, penetrating the bulk of the water, Fig. 11b. The vapor jet moved, and the space that it occupies increased. In this case an unstable annular flow mode was observed, Fig. 11c. After some time the annular flow mode began to disappear, Fig. 11d. As a result, blocking does not take place in the micro-channels, as expected. However, even when the boiling occurred at the central part of a micro-channel, the vapor was accumulated also in the inlet plenum. This result agrees with previous experimental studies. As is pointed out by Peng and Wang (1998) the study of the flow boiling in triangular micro-channels showed that vapor phase was present in the inlet collector.

In the central part and close to the outlet plenum of the channels, depending on heat flux and liquid velocity, the regimes "vapor with clusters of droplets" and "vapor with a thin liquid layer" were observed. In Fig. 12 two-phase steam–water flow in the central part of the parallel micro-channels is displayed. It is the top view observed through transparent cover. The field of view is 2.4 mm in the streamwise direction and 2.0 mm in the spanwise direction, the flow moves from left to right. In these images three micro-channels are shown, marked by gray color or by gray color with the light and dark regions. In the channels A and B, clusters of liquid droplets were observed, Fig. 12a. One of the conclusions of the study is the extreme brevity of the time during which the presence of "vapor with clusters of droplets" regime was observed. The clusters may appear as on the corner of the bottom as on the side-walls (Fig. 12a, channel A). After a time interval of 0.01 s, the liquid drops were not observed on the bottom of channel B, Fig. 12b. Fig. 12c shows no presence of liquid droplets in both channels.

Pressure drop fluctuation. As reviewed and discussed by Peng and Wang (1998), heat transfer to liquids in micro-channels is quite different from that for conventional-sized channels. In particular, bubbles cause a significant volume change (relative to the channel). As a result, pressure fluctuations were observed. The temporal behavior of the pressure drop is shown in Fig. 13. The data were obtained at $q = 220$ kW/m^2 and $U_{LS} = 0.14$ m/s. Such a behavior is a result of vapor formation in each micro-channel.

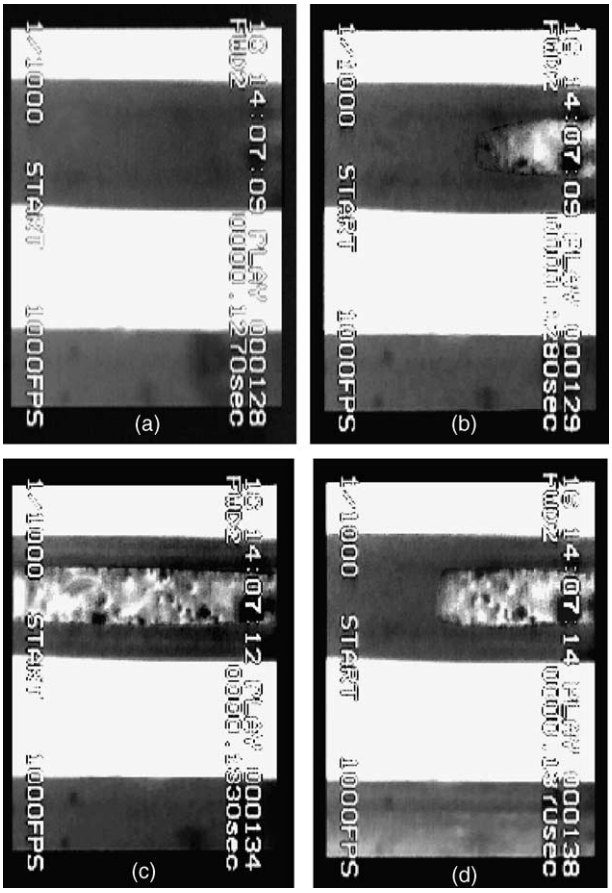

Fig. 11. Flow pattern near the inlet collector. $U_{LS} = 0.14$ m/s, $q = 220$ kW/m^2. Type A plenum.

Temperature distribution on the heated wall. The experimental results of flow visualization suggest that unstable regions occur in two-phase flow in parallel channels. These are important conclusions, but they provide no clarification of how these regions affect temperature distribution on the side of a heater. Although the present study includes the hydraulic aspects of the problem, it relates primarily to the heater side problem. In physical objects including thermal and fluid flow systems, the conjugate problem in terms of heater, how the heater is represented, and boiling as a local-instantaneous problem, should be considered. The issue of temperature variations on the chip surface is a key characteristic of such a problem.

The temperature distribution on the heated wall depends on the material and design of the module, flow rate into the micro-channels and the heat flux. For a given values of flow rate and heat flux, the infrared (IR) image of the heated module side was clearly observed. For example, the typical IR images of the heated side of the module 2 are shown in Figs. 14 and 15. The area of the heater is marked as a square, the flow moved from right to left. We restricted the thermal image analysis to the marked square area of 10×10 mm. The temperature distribution on the heated wall and the histogram of the thermal field at $q = 190$ kW/m^2 and $U_{LS} = 0.14$ m/s are

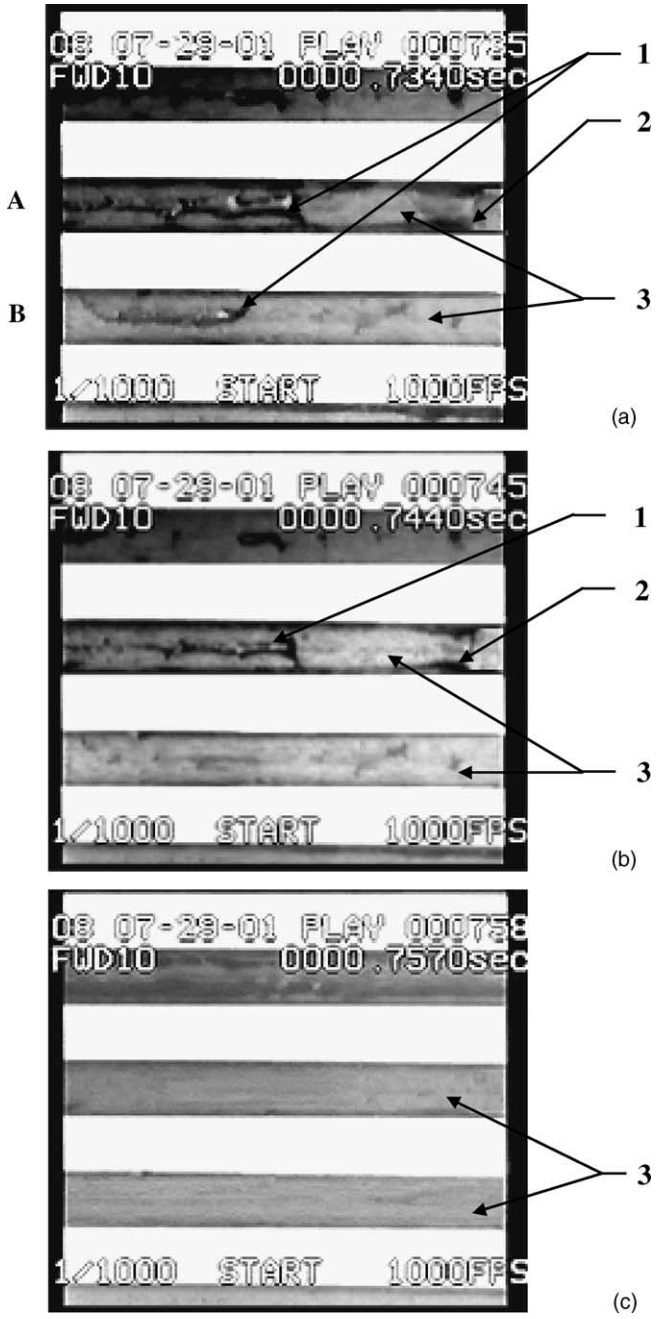

Fig. 12. Boiling in the central part of micro-channels. $U_{LS} = 0.14$ m/s, $q = 220$ kW/m^2. Type A plenum: 1—clusters of liquid droplets on the bottom of the channel; 2—clusters of the liquid droplets on the side-wall of the channel; 3—steam.

shown in Fig. 14a and b, respectively. In this case the mean temperature (averaged over the surface of the heater was of $T_{mean} = 93.3$ °C and boiling was observed in part of the parallel micro-

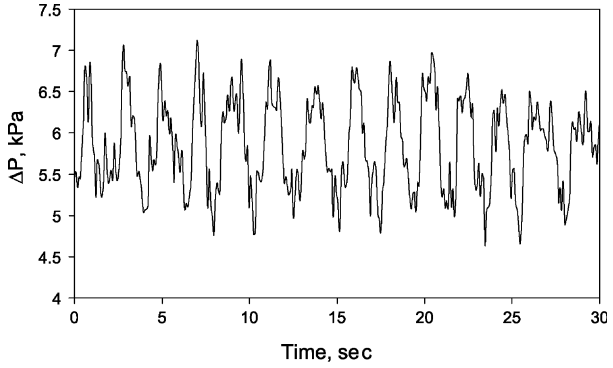

Fig. 13. Pressure drop fluctuations. $U_{LS} = 0.14$ m/s, $q = 220$ kW/m^2. Type B plenum.

channels only. The temperature measurements performed simultaneously with flow visualization, allowed us to conclude that convective boiling in part of the micro-channels took place, when $T_{mean} < T_S$ (T_S is the saturation temperature). When $T_{mean} > T_S$ boiling in all parallel micro-channels was observed. The temperature distribution on the heated wall and the histogram of the thermal field at $T_{mean} = 104.1$ °C, $q = 220$ kW/m^2 and $U_{LS} = 0.14$ m/s are shown in Fig. 15a and b, respectively. From Figs. 14 and 15 one can conclude that the variation of $(T_{max} - T_S)$ is more than 20 K, where T_{max} is the maximum temperature on the heated surface. It is clear that consideration of boiling curve and flow regimes in parallel micro-channels should take into account such a wide variation of wall temperature.

Boiling curve. Previous investigators (Johansen, 1991; Hong et al., 1997) have plotted, for convective boiling in single large size tube, the heat flux vs. wall superheat $(T_{mean} - T_S)$, where T_{mean} is the mean temperature on the heated surface. In the present study the results considered above show that the difference $(T_{mean} - T_S)$ may be negative. That is why we use the difference $(T_{max} - T_S)$. In Fig. 16 the dimensionless heat flux q^* is plotted vs. the difference $(T_{max} - T_S)$. Dimensionless heat flux is defined as $q^* = (q/\dot{m}C_p\Delta T)(T_{max}/T_{mean})$, where q is the heat flux, C_p is the specific heat, $\Delta T = T_S - T_0$, T_S is the saturation temperature, T_0 is the water temperature supplied to the inlet collector, T_{max} and T_{mean} are maximum and average temperature of the heated surface, respectively. The term $(q/\dot{m}C_p\Delta T)$ reflects the effect of subcooling. The experimental results of flow visualization suggest that for different number of micro-channels, connected to the inlet and outlet collectors (type A or type B) the same flow patterns occur in the two-phase region. These are important conclusions, but they provide no clarification of how the connection affects the temperature distribution on the heater side. Although the present study includes the hydraulic aspects of the problem, it relates primarily to the heater side problem. In physical objects including thermal and fluid flow systems, the conjugate problem in terms of heater, how the heater is represented, and boiling as a local-instantaneous problem, should be considered. The issue of temperature variations on the chip surface is a key characteristic of such problem. The term (T_{max}/T_{mean}) reflects the non-uniform temperature distribution on the heated surface. In Fig. 16 two regions of convective boiling may be distinguished. In region A the value of $(T_{max} - T_S) < 20$ K and boiling was observed in part of the parallel micro-channels only. It may be referred to low heat flux region. Region B, shown in Fig. 16, may be referred to as high-heat flux region, in this case $(T_{max} - T_S)$ exceeds 20 K.

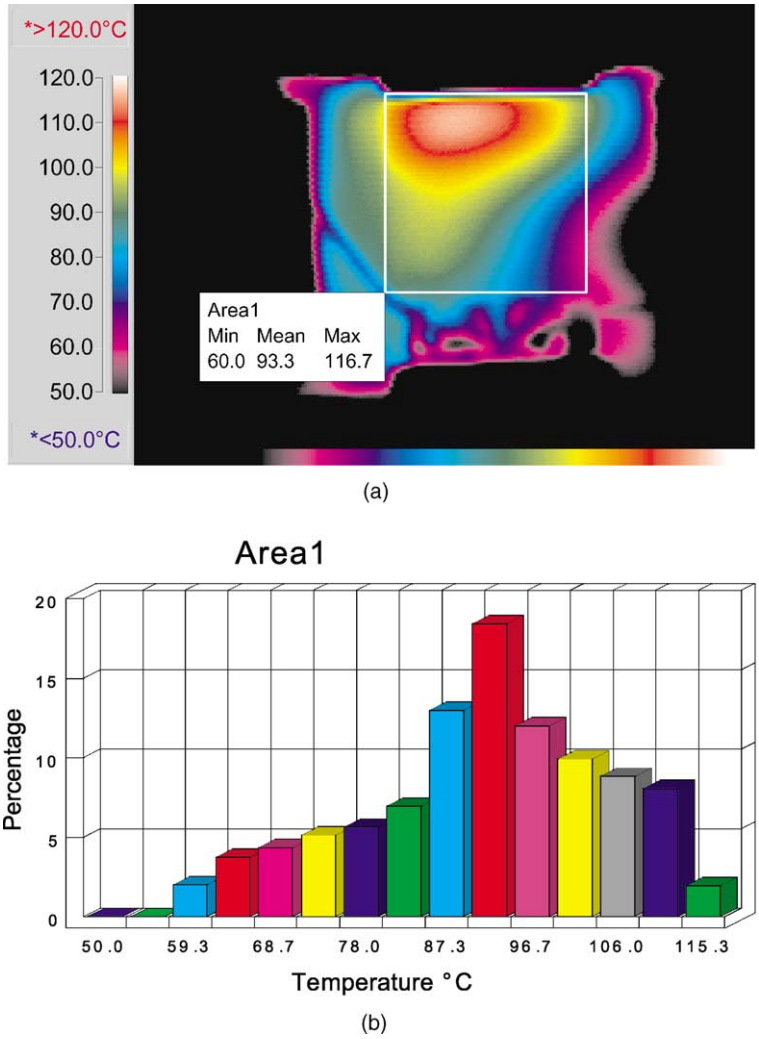

Fig. 14. Thermal field on the heated wall. $U_{LS} = 0.14$ m/s, $q = 190$ kW/m^2. Type B plenum: (a) infrared image (b) histogram of temperature distribution.

Flow regimes map. The low heat flux region is characterized by the presence of liquid phase in all micro-channels of the test module. High values of heat flux region are characterized by vapor generation in all micro-channels and periodical rewetting and refilling of the micro-channels of the test module. In general, the term dryout indicates local contact of the gas phase with the surface. The term used in the present study of the flow visualization is defined with respect to temporal viewpoint of the process time. Observations of different flow behavior at the $(T_{max} - T_S) < 20$ and $(T_{wmax} - T_S) > 20$ lead to the conclusion that the heat transfer mechanism in two regions would be different. Flow rates, heat flux, local surface temperature variations and subcooling affect the value of $(T_{max} - T_S)$. For transition from low heat flux region characterized by continuous liquid phase to high flux region characterized by dryout phenomenon we suggest:

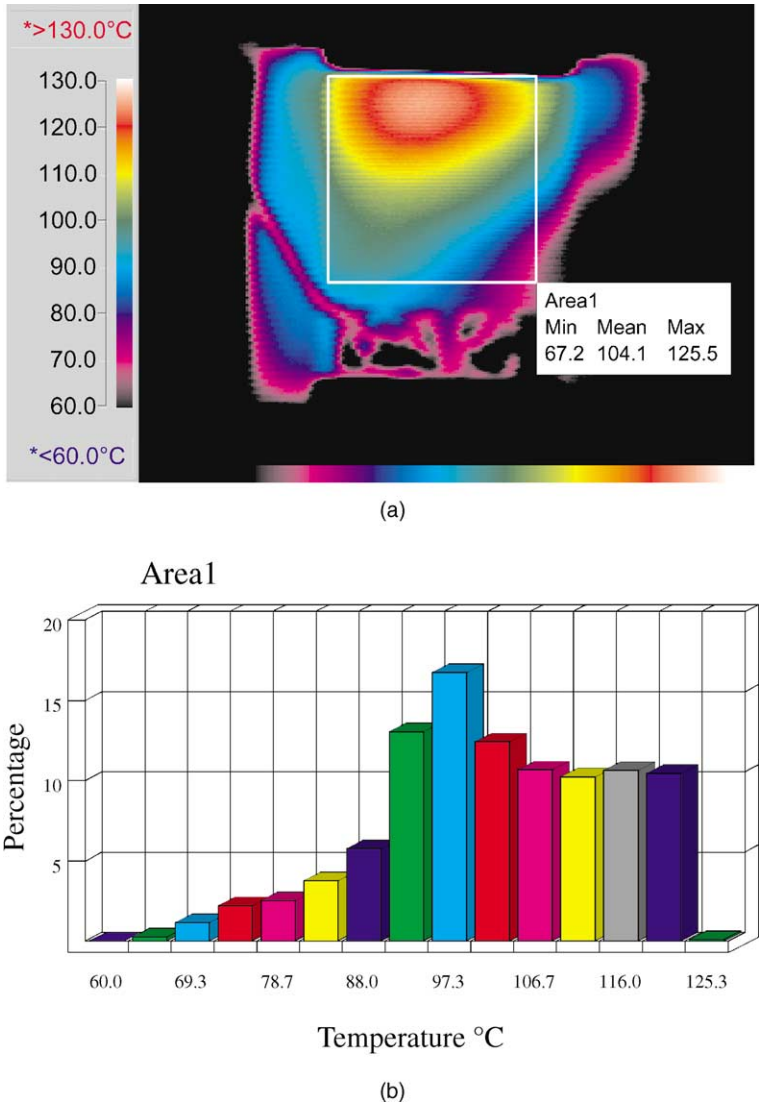

Fig. 15. Thermal field on the heated wall. $U_{LS} = 0.14$ m/s, $q = 220$ kW/m^2. Type B plenum: (a) infrared image (b) histogram of temperature distribution.

Reynolds number $Re = U_{LS}D_h/v$ and dimensionless heat flux q^*, where D_h is the hydraulic diameter, U_{LS} is the superficial liquid velocity in the micro-channel and v is the kinematic viscosity.

In Fig. 17 we present the flow regime map for the three tested modules with triangular parallel micro-channels. The map was obtained for heat fluxes in the range 5.1–50 W/cm^2, and vapor quality in the range 0.01–0.1. The above discussion shows that it is difficult to make meaningful comparison between the present map and previous studies because most previous work have been concerned with flow patterns air–water flow in single tube.

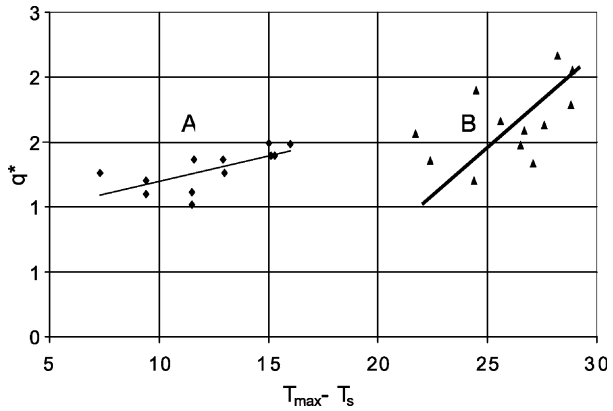

Fig. 16. Boiling curve for parallel micro-channels: A—low heat flux region, B—high-heat flux region.

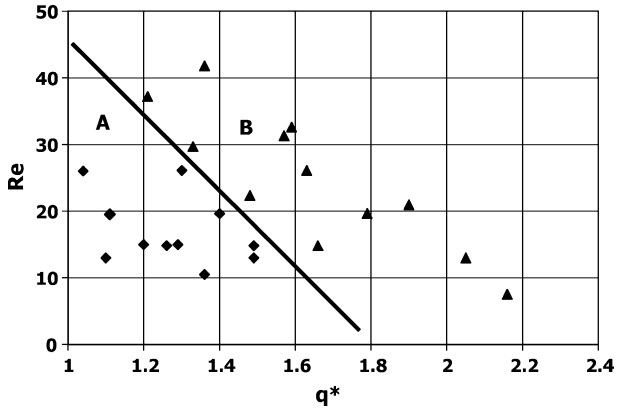

Fig. 17. Flow regime map: A—low heat flux region, B—high-heat flux region.

4. Conclusions

We studied air–water and steam–water two-phase flow in three test modules with triangular parallel micro-channels. The images of two-phase flow patterns, as well as the measured temperatures on the heated surface, have been analyzed.

In air–water flow the different flow pattern occur simultaneously in different micro-channels. Although the gas core may occupy almost the entire cross-section of the triangular channel, making the side-walls partially dry, the liquid phase always remained continuous due to the fact that the liquid was drawn into the triangular corners by surface tension.

Unlike flow pattern in air–water flow, experiments have shown the explosive bubble behavior in steam–water flow. The bubble nucleation was investigated, the bubble size and the velocity of bubble motion was measured.

Two flow regimes may be considered in steam–water flow. The low heat flux region is characterized by the presence of liquid phase in part of the parallel micro-channels. In this case the mean temperature on the whole heated surface is less than the saturation temperature of the fluid.

At low heat fluxes, bubble nucleation on the wall occurred. The smallest bubbles were on the order of 30 μm. These bubbles, like small bubbles observed by Jiang et al. (2001), grew and were swept downstream in the micro-channels. The high of heat flux region is characterized by convective boiling, in all parallel micro-channels, accompanied by quasi-periodical rewetting and refilling of the micro-channels. At high-heat fluxes the vapor was accumulated also in the inlet plenum. At inception, the bubble is close to being spherical. Then the bubbles extend and occupy the entire cross-section of the channel, like vapor slugs. The velocity of the vapor slugs is higher than the velocity of surrounding fluid. We assume that the bubbles respond to an initial brief but large increase in the internal pressure. Therefore, after the first moments during which the pressure is still high, there is a rapid change of the bubble volume. Then the internal pressure quickly falls to near the saturation value, due to the expansion. In this case the bubble size approach an asymptotic value. This situation takes place at low values of heat flux only. Figs. 7–9 show the bubble growth, temporal variation of vapor bubble size, and velocity of bubble tail, respectively. The situation changes drastically at high value of heat flux. In this case the heat transferred to the vapor volume is higher and the explosive vaporization and significant pressure drop fluctuations occur, Figs. 11 and 12. Flow pattern, observed in the present study and reported also by Kandlikar (2002), revealed a flow reversal in some channels with expanding bubbles pushing the liquid–vapor interface in both upstream and downstream directions.

Acknowledgements

This research was supported by the Fund for Promotion of Research at the Technion. A. Mosayk is supported by a joint grant from the Center for Absorbtion in Science of the Ministry of Immigrant Absorbtion and the Committee for Planning and Budgeting of the Council for Higher Education under the framework of the KAMEA PROGRAM, and E. Pogrebnyak was supported by the Center for Absorption in Science, Ministry of Immigrant Absorption State of Israel.

References

Bibeau, E.L., Salcudean, M., 1994. A study of bubble ebullition in forced-convective subcooled nucleate boiling at low pressure. Int. J. Heat Mass Transfer 37, 2245–2259.

Damianides, C.A., Westwater, J.W., 1988. Two-phase flow patterns in a compact heat exchanger and in small tubes. In: Proceedings of the Second UK National Conference on Heat Transfer, Glasgow, 14–16 September. Mechanical Engineering Publications, London, pp. 1257–1268.

Fukano, T., Kariyasaki, A., 1993. Characteristics of gas–liquid two-phase flow in capillary. Nucl. Eng. Des. 141, 59–68.

Ghiaasiaan, S.M., Abdel-Khalik, S.I., 2001. Two-phase flow in micro-channels. Adv. Heat Transfer 34, 145–253.

Hetsroni, G., Mosyak, A., Segal, Z., 2001. Nonuniform temperature distribution in electronic devices cooled by flow in parallel micro-channels. IEEE Trans. Components Packag. Technol. 24, 16–23.

Hong, Y.S., Ammerman, C.N., You, S.M., 1997. Boiling characteristics of cylindrical heaters in saturated, gas saturated, and pure-subcooled FC 72. J. Heat Transfer 119, 313–318.

Jiang, L., Wong, M., Zohar, Y., 2001. Forced convection boiling in a micro-channel heat sink. J. Microelectromech. Sys. 10, 80–87.

Johansen, K., 1991. Low quality transition and inverted annular flow film boiling of water: an updated review. Exp. Thermal Fluid Sci. 4, 497–509.

Kandlikar, G., 2002. Fundamental issues related to flow boiling in minichannels and micro-channels. Exp. Thermal Fluid Sci. 26, 389–407.

Kennedy, J.E., Roach Jr., G.M., Dowling, M.F., Abdel-Khalik, S.I., Ghiaasiaan, S.M., Jeter, S.M., Quershi, Z.H., 2000. The onset of flow instability in uniformly heated horizontal micro-channels. J. Heat Transfer 122, 118–125.

Lowe, D.C., Rezkallah, K.S., 1999. Flow regime identification in microgravity two-phase flows using void fraction signals. Int. J. Multiphase Flow 25, 433–457.

Ory, E., Yuan, H., Prosperetti, A., Popinet, S., Zaleski, S., 2000. Growth and collapse of a vapor bubble in narrow tube. Phys. Fluids 12, 1268–1277.

Ozawa, M., Akagawa, K., Sakaguchi, T., Tsukahara, T., Fujii, T., 1979. Oscillatory flow instabilities in air–water two-phase flow systems. Report. Pressure drop oscillation. Bull. JSME 22, 1763–1770.

Ozawa, M., Akagawa, K., Sakaguchi, T., 1989. Flow instabilities in parallel-channel flow systems of gas–liquid two-phase mixtures. Int. J. Multiphase Flow 15, 639–657.

Peng, X.F., Hu, H.Y., Wang, B.X., 1998. Boiling nucleation during liquid flow in micro-channels. Int. J. Heat Mass Transfer 41, 101–106.

Peng, X.F., Wang, B.X., 1998. Forced convection and boiling characteristics in micro-channels. In: Proceedings of 11 IHTC, Kyonji, Korea, August 23–28, vol. 1, pp. 371–390.

Prodanovic, V., Fraser, D., Salcudean, M., 2002. Bubble behavior in subcooled flow boiling of water at low pressures and flow rates. Int. J. Multiphase Flow 28, 1–19.

Qu, W., Mudawar, I., 2002. Prediction and measurement of incipient boiling heat flux in micro-channel heat sinks. Int. J. Heat Mass Transfer 45, 3933–3945.

Triplett, K.A., Ghiaasiaan, S.M., Abdel-Khalik, S.I., Sadowski, D.L., 1999. Gas–liquid two-phase flow in micro-channels. Part 1: two-phase flow patterns. Int. J. Multiphase Flow 25, 377–394.

Tshuva, M., Barnea, D., Taitel, Y., 1999. Two-phase flow in inclined parallel pipes. Int. J. Multiphase Flow 25, 1491–1503.

Zhang, L., Ko, J.M., Jiang, L., 2002. Measurements and modeling of two-phase flow in micro-channels with nearly constant heat flux boundary conditions. J. Microelectromech. Sys. 11, 12–19.

Zhao, T.S., Bi, Q.C., 2001. Co-current air–water two-phase flow patterns in vertical triangular micro-channels. Int. J. Multiphase Flow 27, 765–782.